

Biocompatibility of polyetheretherketone for the treatment of orbital bone defects

Rui-Dong Gu, Fan Xiao, Lin Wang, Kai-Jian Sun, Lin-Lin Chen

Department of Ophthalmology, the Fourth People's Hospital of Shenyang, Shenyang 110031, Liaoning Province, China

Correspondence to: Lin-Lin Chen. Department of Ophthalmology, the Fourth People's Hospital of Shenyang, Shenyang 110031, Liaoning Province, China. cllnn@hotmail.com
Received: 2020-02-05 Accepted: 2020-03-19

Abstract

• **AIM:** To investigate the biocompatibility and therapeutic effects of polyetheretherketone (PEEK) on recovery of a rabbit orbital defect.

• **METHODS:** Totally 16 New Zealand rabbits were used to establish an orbital bone defect model and then randomly divided into two groups. PEEK was implanted in the experimental group. The control group was blank, and no substance was implanted. The model rabbits were sacrificed at 4 and 8wk, and examined by general observations, histology, electron microscopy, Western blotting, and real-time polymerase chain reaction.

• **RESULTS:** No infection or rejection occurred after PEEK implantation, and biocompatibility was good. The relative expression of vascular endothelial growth factor (VEGF) protein in the experimental group was significantly higher than that in the control group postoperatively ($P < 0.05$). Bone defect repair in the experimental group was significantly better than that in the control group in the same period and some osteogenesis was observed.

• **CONCLUSION:** PEEK has good biocompatibility and efficacy for the treatment of orbital bone defects in a rabbit model.

• **KEYWORDS:** polyetheretherketone; histocompatibility; orbital defect; orbital burst fracture; three-dimensional printing; rabbit

DOI: 10.18240/ijo.2020.05.05

Citation: Gu RD, Xiao F, Wang L, Sun KJ, Chen LL. Biocompatibility of polyetheretherketone for the treatment of orbital bone defects. *Int J Ophthalmol* 2020;13(5):725-730

INTRODUCTION

Orbital blowout fracture results from external forces acting on the eye and causing a sudden increase in orbital pressure. This leads to rupture of the orbital bone wall

in the weak part of the eye, orbital wall defects, ocular nerve injury, soft tissue incarceration or herniation, enophthalmos, diplopia, and eye movement disorders. Imaging examination indicates that the orbital contents are obviously incarcerated or herniated from the defect area of the orbital wall, and there are clinical manifestations of the eyes, which should be treated surgically^[1]. Because the scope and circumstances of fractures vary from case to case, the ideal approach is to use three-dimensional (3D) printing technology to create individualized repair materials for surgical treatment. 3D printing technology has been widely used in the medical field, and there are many types of printing matrix materials. One of the most widely used materials for the treatment of bone defects is polyetheretherketone (PEEK)^[2]. PEEK has shown strong development momentum in the field of biomedical materials because of its excellent wear resistance, good magnetic penetration, antioxidant properties, biocompatibility, easy processing and molding, light weight, and elastic modulus close to cortical bone^[3-5]. 3D-printed PEEK has been applied to orthopedics, stomatology, neurosurgery, and other disciplines^[6-10], and has been rarely reported to be applied to orbital bone defects. In our study, 3D-printed PEEK implants were implanted into an animal model of orbital fracture, and biocompatibility and curative effects were observed to provide an experimental basis for the selection and application of clinical orbital wall reconstruction materials.

MATERIALS AND METHODS

Ethical Apporval All treatments on rabbits were in accordance with the guidelines of the Chinese Ministry of Science and Technology Guidelines on the Humane Treatment of Laboratory Animals and the Association for Research in Vision and Ophthalmology (ARVO) Statement for the Use of Animals in Ophthalmic and Vision Research.

Experimental Materials Sixteen healthy adult New Zealand rabbits, male or female weighing 2.5-3.0 kg and 4-6mo of age, were provided by the Experimental Center of China Medical University. PEEK implants were obtained from Electro Optical Systems (Munich, Germany). A Western blot kit for vascular endothelial growth factor (VEGF) was obtained from Bioss (Massachusetts, USA). A VEGF real-time polymerase chain reaction kit was obtained from BioTeke (Beijing, China). A CT-GE revolution 256 was purchased from GE (Boston,

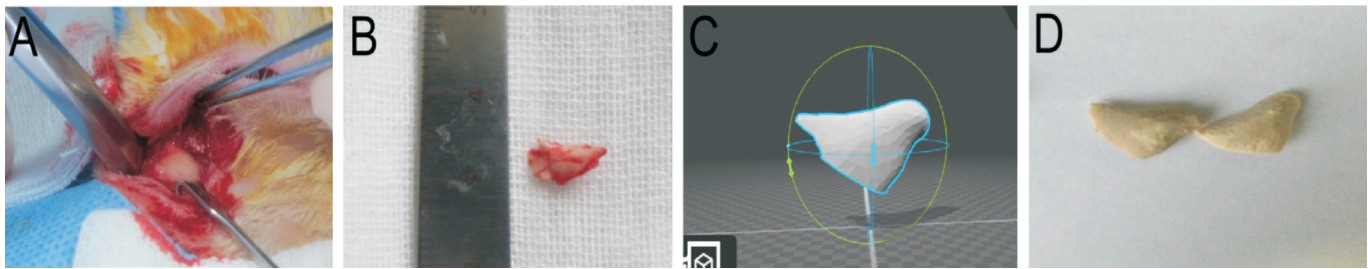


Figure 1 Production of PEEK implants A: Establishment of the orbital bone defect model in rabbits; B: Part of the orbital bone was removed; C: 3D data were obtained by CT scanning; D: PEEK implants printed by 3D printing technology.

Massachusetts, USA). The SU3500 scanning electron microscope was obtained from Hitachi China (Beijing, China). A fluorescence quantifier Exicycler™ 96 was purchased from BIONEER (Daejeon, Korea). ECL was obtained from Thermo Fisher Scientific (Waltham, MA, USA).

Experimental Methods

Animal grouping Sixteen New Zealand white rabbits were randomly divided into two groups. After the orbital bone defect model was established according to the PEEK implant shape. The control group was the blank, and no substance was implanted. In the experimental group, PEEK was implanted in the bone defect area.

Production of polyetheretherketone implants Before the operation, the animals were deprived of water, and 3% pentobarbital sodium solution (30 mg/kg) was injected into the ear margin under general anesthesia. A 1.5-cm arc incision was made at the orbital margin of the lower eyelid, the skin and subcutaneous tissue were incised, the flap was pulled with claw hooks, the orbital periosteum was exposed bluntly, and the periosteum was incised. The orbital bone was exposed, 1 cm outside of the inferior orbital rim was measured with a caliper, and the bone within the range was removed with a rongeur and subjected to CT scanning to obtain 3D data. Then, the PEEK implants were prepared using 3D printing technology. Because the aim of this study was to assess biocompatibility and it would require a lot of time and high costs to prepare specific PEEK implants for multiple rabbits, we prepared PEEK implants based on the first rabbit orbital bone defect model (Figure 1).

Model establishment The preparation was performed as described above. According to the PEEK implant shape, part of the orbital bone was removed to establish the animal model of the orbital bone defect. In the experimental group, a sterile PEEK implant was implanted into the orbital bone defect area and fixed with biological glue. The incision was washed with normal saline, and then the wound was sutured with 6-0 absorbable suture and bandaged with sterile gauze. The control group were sutured directly. For post-operative management, animals were administered an intramuscular injection of antibiotics (5 mg/kg gentamicin, once a day for 3d)

and tobramycin eye drops (three times a day for 7d) to prevent infection.

General observations Post-operative inflammatory reactions around the wound and wound healing were observed every day, including whether there was infection and the implant was rejected, and changes in appearance.

Gross specimen observations After the operation, samples were obtained at weeks 4 and 8. The skin around the orbit was incised along the eyelid, the subcutaneous tissue was separated, the bony orbital margin was exposed, and the reaction around the PEEK implant and surrounding tissues was observed.

Hematoxylin-eosin and Sirius red staining Immediately after PEEK implants and surrounding tissues were removed, they were fixed in 4% paraformaldehyde for 24h. Then, the specimens were prepared and examined by two pathological investigators who performed dehydration and clearing steps. The paraffin-embedded tissues blocks were serially cut into 7- μ m thick sections, applied to glass slides, and then dried at 65°C for 2h. They were then placed in xylene for 10min twice to remove the paraffin, and then transferred to serial concentrations of ethanol to remove the xylene (100%, 95%, 80%, and 70% ethanol for 5min each). We stained the sections with hematoxylin (H&E Stain Kit; Solarbio, Beijing, China) for 5min and then rinsed them with warm tap water for 3min to remove the hematoxylin. Then, we placed the sections in eosin containing 0.01% HCL for 1min, and finally rinsed them with tap water for 10min. We mounted the sections with Permunt™ mounting medium (ZSGB-BIO Corp., Beijing, China) and covered them with coverslips. Similarly, we performed Sirius red staining according to the manufacturer's protocols.

Electron microscopy Immediately after PEEK implants and surrounding tissues were removed, the specimens were fixed in 2.5% glutaraldehyde for 2h, repeatedly rinsed, and then fixed in 1% osmium acid for 2h. The samples were placed in acetone at 30%, 50%, 70%, 80%, 90%, and 95% for 10min each, and 100% acetone for three times for 15min each. The specimens were placed in a mixture of acetone and equivalent epoxy resin for 2h, and then embedded in a pure epoxy resin overnight at room temperature. After ultrathin sectioning, the specimens were observed by scanning electron microscopy.

Western blotting The surrounding tissue of the bone defect was collected, and a tissue lysate was prepared. After 30min of lysis, the sample was centrifuged at 10 000 rpm for 10min at 4°C. The supernatant was collected to obtain the total protein. Protein concentrations were determined using the BCA kit. After protein loading, SDS-PAGE was performed for 2.5h, and then proteins were transferred for 1.5h. The primary anti-VEGF antibody was applied at 4°C overnights. Then, sheep anti-rabbit IgG-HRP as the secondary antibody was applied at 37°C for 45min. ECL chemiluminescence reagent was added to the PVDF membrane, followed by analysis in the gel imaging system. Then, stripping solution was added to the PVDF membrane, and distilled water was used for repeated rinsing. An antibody against β -actin as the internal reference was applied at 4°C overnights, and then sheep anti-rabbit IgG-HRP as the secondary antibody was applied at 37°C for 45min. ECL chemiluminescence reagent was added to the PVDF membrane, followed by analysis in the gel imaging system. The membrane was scanned, and the optical density of the bands was analyzed by gel-pro-analyzer software.

Real-time polymerase chain reaction The surrounding tissue of the bone defect was collected, RNA was extracted, and cDNA was synthesized using the reverse transcription kit. The housekeeping gene β -actin served as the internal control. The oligonucleotide primers used were as follows: VEGF F: ATGGCAGAAGAAGGAGACA; VEGF R: CGCAGGAAGGCTTGAATAT; β -actin F: CCCATCTACGAGGGCTACGC; β -actin R: TCCTTGATGTC CCGCACGAT. Each experiment was repeated at least three times.

Statistical Analysis Data were analyzed using SPSS (Version 19.0; IBM, Armonk, New York, USA). Measurement data are expressed as the mean \pm standard deviation (SD). Comparisons between the model and control groups were made by the paired *t*-test. Data that did not meet the normal distribution were tested by the paired rank test. $P < 0.05$ was considered to be statistically significant.

RESULTS

General Conditions There were no post-operative infections or deaths of all animal models and no implant shedding, all of which entered the experimental analyses.

General Morphological Observations At week 4 after the operation, periosteum covered a part of the PEEK implant surface in the experimental group. The bone defect in the control group was obvious without healing. At week 8 after the operation, the PEEK implant surface was covered and enveloped by periosteum in the experimental group and healing well with the fracture end without inflammation or rejection (Figure 2). The bone defect in the control group was still obvious without osteogenesis.



Figure 2 In the experimental group, the PEEK implant (black arrow) was covered with periosteum and soft tissue at week 8 after the operation (abaxial view).

Hematoxylin-Eosin Staining At week 4 after the operation, bone tissue in the bone defect area was sparse and mainly fibrous (Figure 3A). The periosteum covered a part of the PEEK implant surface in the experimental group without inflammation or rejection, and a small number of osteoblasts was observed (Figure 3B). At week 8 after the operation, there was no obvious healing in the control group, and the bone defect was obvious (Figure 3C). The PEEK implant surface in the experimental group was covered with periosteum and soft tissue without inflammation or rejection, and osteoblasts had increased gradually (Figure 3D).

Sirius Red Staining At week 4 after the operation, the bone defects in the control group were sparsely stained and arranged irregularly (Figure 4A). Compared with the control group, the experimental group showed more staining and more even staining (Figure 4B). At week 8 after the operation, the bone defect area in the control group was increased slightly compared with week 4 after the operation (Figure 4C). Compared with the control group, the experimental group had more staining, more uniform staining, a more regular arrangement than the control group (Figure 4D).

Scanning Electron Microscopy At week 4 after the operation, the bone defect in the control group was exposed without healing (Figure 5A). In the experimental group, a part of the PEEK implant surface was covered by periosteum without rejection (Figure 5B). At week 8 after the operation, the bone defect in the control group showed no obvious healing, and a part of the bone defect was covered by fibrous tissue (Figure 5C). The PEEK implant surface in the experimental group was covered by periosteum and soft tissue with close connection, good biocompatibility, and no rejection (Figure 5D).

Western Blotting At week 4 after the operation, the relative expression of VEGF protein in the experimental group was significantly higher than that in the control group ($P < 0.05$). At week 8 after the operation, the relative expression of VEGF

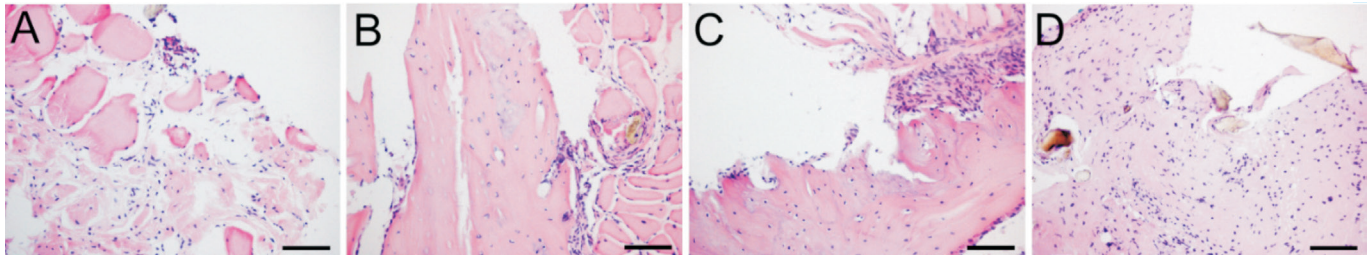


Figure 3 H&E staining (×200) A: At week 4 after the operation, there was no healing in the control group; B: At week 4 after the operation, periosteum covered a part of the PEEK implant surface in the experimental group; C: At week 8 after the operation, the bone defect showed no obvious healing; D: At week 8 after the operation, the PEEK implant surface in the experimental group was covered with periosteum and soft tissue without inflammation or rejection, and osteoblasts had increased gradually.

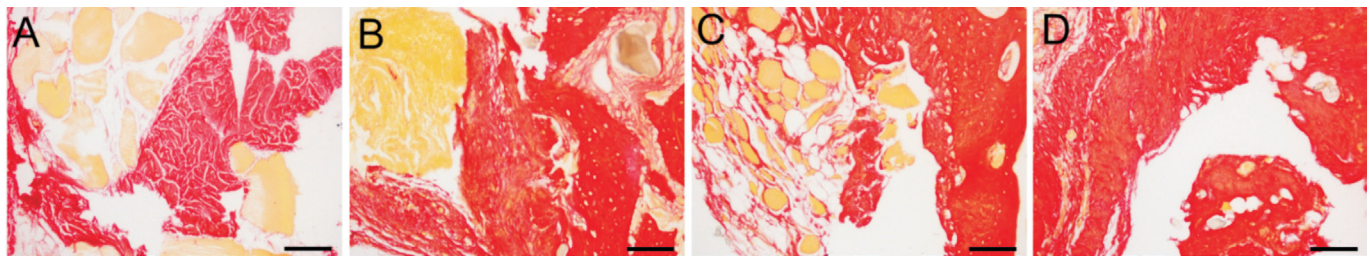


Figure 4 Sirius red staining (×200) A: At week 4 after the operation, bone defects in the control group were stained sparsely and arranged irregularly; B: At week 4 after the operation, compared with the control group, the experimental group showed more staining and more even staining; C: At week 8 after the operation, the bone defect area in the control group was increased slightly compared with week 4 after the operation; D: At week 8 after the operation, the experimental group had more staining, more uniform staining, a more regular arrangement compared with the control group.

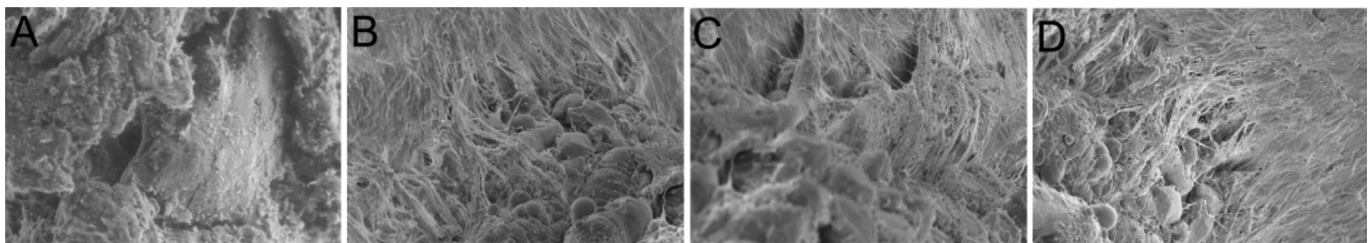


Figure 5 Scanning electron microscopy (×320) A: At week 4 after the operation, the bone defect in the control group was exposed without healing; B: At week 4 after the operation, part of the PEEK implant surface was covered by periosteum without rejection; C: At the week 8 after the operation, the bone defect in the control group showed no obvious healing; D: At week 8 after the operation, the PEEK implant surface in the experimental group was covered by periosteum and soft tissue with close connection, good biocompatibility, and no rejection.

protein in the experimental group was also significantly higher than that in the control group ($P < 0.05$; Figure 6).

Real-time Polymerase Chain Reaction At week 4 after the operation, relative expression of VEGF mRNA in the experimental group was significantly higher than that in the control group ($P < 0.05$). At week 8 after the operation, relative expression of VEGF mRNA in the experimental group was also significantly higher than that in the control group ($P < 0.05$).

DISCUSSION

A defect of the orbital bone wall is caused by orbital blowout fracture. To restore the continuity of the bone wall and avoid a series of clinical symptoms caused by incarceration or herniation of the orbital contents, it is necessary to reconstruct the defect site. The effect of reconstruction depends on the

choice of surgical plan and repair materials^[11]. Accurate surgical anatomy and proper fracture reduction are critical for the recovery of orbital anatomy and functions^[12]. Because the scope and circumstances of fractures vary from case to case, the ideal approach is to use 3D printing to create personalized repair materials for surgical treatment, especially for severe orbital blowout fractures. Recent studies^[13-14] show that 3D printing combined with endoscopy improve diplopia, eye movement disorder, and eye depression. All patients underwent routine preoperative CT examination, and 3D printing technology based on the CT data produced a proportional model of the orbital fracture, and a titanium mesh was prepared based on the model, which was not only more accurate, but also reduced the operation time and steps. Other studies^[15-17]

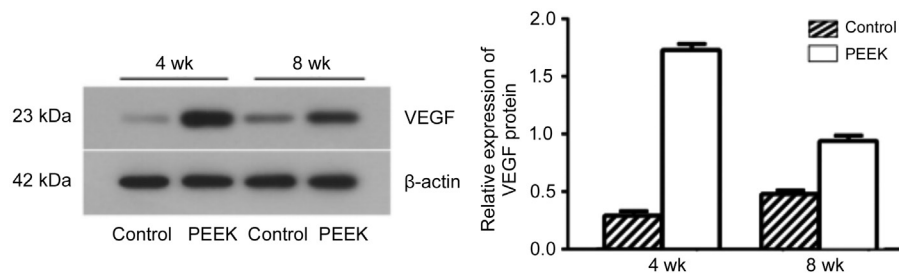


Figure 6 Western blotting Relative expression of VEGF protein in the experimental group was significantly higher than that in the control group in the same period ($P < 0.05$).

support that 3D-printed models of orbital fractures provide personalized anatomical information that can help guide and plan surgical procedures. 3D printing technology is widely used in the medical field and has become a research hotspot. It is not only applied to simulation model manufacturing as mentioned above, but also applied to orthopedic instruments, orthopedic implants, tissue engineering stents, and drug development^[18]. 3D printing technology involves a variety of organ systems in the body, including bones, muscles, nerves, lymph, endocrine, reproductive, skin, respiratory, digestive, urinary, and circulatory systems^[19].

General morphological observations and HE staining showed that PEEK implant biocompatibility was good with no rejection or infection in the experimental group. At week 8 after the operation, the PEEK implant surface in the experimental group was covered with periosteum, and the fracture had healed well. However, in the bone defect area of the control group, bone tissue was sparse with no obvious healing and a small amount of covering fibrous tissue, which was consistent with the results of Cheng *et al*^[20]. Sirius red mainly stains type I collagen. Oh *et al*^[21] showed that type I collagen fibers affect the growth, adhesion, and mineral synthesis ability of osteoblasts, thereby affecting the arrangement of collagen fibers and minerals in bone and affecting the mechanical properties of bone. Our study showed that type I collagen increased gradually over time in both groups. Compared with the control group in the same time period, the experimental group had more staining, more uniform staining, a more regular arrangement, and even distribution near the PEEK implant, which was consistent with the results of Cao *et al*^[22].

The scanning electron microscopy showed that the bone defect was repaired faster and more obviously in the experimental group than in the control group. At week 8 after surgery, there was no obvious healing trend in the bone defect area of the control group, and fibrous tissue covered part of the bone defect. The surface of PEEK implant in the experimental group was covered by periosteum and soft tissue, with close connection, good histocompatibility and no rejection.

In our study, the effect of the bone defect treatment in the experimental group was significantly better than that in the

control group. Therefore, we measured the level of VEGF, which plays an important role in bone defect repair. The fracture healing process is largely driven by VEGF^[23]. From the initial concentration in the fracture hematoma to the final remodeling stage to promote bone transformation, VEGF is involved in many steps of the whole fracture healing process^[24-25]. Geiger *et al*^[26] showed that expression of VEGF increases in the process of fracture healing and vascular reconstruction. VEGF is related to angiogenesis at the fracture end and in fracture healing, which promotes the proliferation of vascular endothelial cells. Becker *et al*^[27] showed that VEGF has a pro-differentiation effect on osteoblasts and mediates autocrine and paracrine actions of osteoblasts and vascular endothelial cells to promote bone formation. In this study, real-time polymerase chain reaction and Western blotting revealed that the relative expression of VEGF protein and mRNA in the experimental group was significantly higher than that in the control group in the same period, indicating that the expression of VEGF was affected by some mechanism after the implantation of PEEK to repair the bone defect, and the high expression of VEGF promoted repair of the bone defect. Al Subaie *et al*^[28] showed that drugs that inhibit the activity of VEGF may inhibit bone healing and osseointegration of the tibia in rats. Further studies^[29-30] have shown that local application of VEGF to a graft in the early stage of fracture healing has a positive effect on fracture recovery.

In summary, PEEK has good biocompatibility and efficacy for the treatment of orbital bone defects in rabbits. After PEEK implantation, the expression of VEGF was higher and fracture repair was promoted. The specific mechanism remains to be studied further.

ACKNOWLEDGEMENTS

Foundation: Supported by the Liaoning Province Natural Science Foundation Guidance Program (No.20170520286).

Conflicts of Interest: Gu RD, None; Xiao F, None; Wang L, None; Sun KJ, None; Chen LL, None.

REFERENCES

- Borad V, Lacey MS, Hamlar DD, Dresner HS, Yadava GK, Schubert W. Intraoperative imaging changes management in orbital fracture repair. *J Oral Maxillofac Surg* 2017;75(9):1932-1940.

- 2 Mao HL, Gu ZW. Development status and trend of bio-3D printed polymer materials. *Materials China* 2018;37(12):949-969.
- 3 Wyatt H, Elliott M, Reville P, Clarke A. The effect of engineered surface topography on the tribology of CFR-PEEK for novel hip implant materials. *Biotribology* 2016;7:22-30.
- 4 Wang L, Weng LQ, Song SH, Zhang ZY, Tian SL, Ma R. Characterization of polyetheretherketone-hydroxyapatite nanocomposite materials. *Materials Science & Engineering: A* 2011;528(10-11):3689-3696.
- 5 Han CM, Lee EJ, Kim HE, Koh YH, Kim KN, Ha Y, Kuh SU. The electron beam deposition of titanium on polyetheretherketone (PEEK) and the resulting enhanced biological properties. *Biomaterials* 2010;31(13):3465-3470.
- 6 Liu D, Fu J, Fan HB, Li DC, Dong EC, Xiao X, Wang L, Guo Z. Application of 3D-printed PEEK scapula prosthesis in the treatment of scapular benign fibrous histiocytoma: a case report. *J Bone Oncol* 2018;12:78-82.
- 7 Mounir M, Shalash M, Mounir S, Nassar Y, El Khatib O. Assessment of three dimensional bone augmentation of severely atrophied maxillary alveolar ridges using prebent titanium mesh vs customized poly-ether-ether-ketone (PEEK) mesh: a randomized clinical trial. *Clin Implant Dent Relat Res* 2019;21(5):960-967.
- 8 Kang JF, Wang L, Yang CC, Wang L, Yi C, He JK, Li DC. Custom design and biomechanical analysis of 3D-printed PEEK rib prostheses. *Biomech Model Mechanobiol* 2018;17(4):1083-1092.
- 9 Zhang JB, Tian WQ, Chen JY, Yu J, Zhang JJ, Chen JC. The application of polyetheretherketone (PEEK) implants in cranioplasty. *Brain Res Bull* 2019;153:143-149.
- 10 Krieg SM, Balsler N, Pape H, Sollmann N, Albers L, Meyer B. Topping-off technique for stabilization of lumbar degenerative instabilities in 322 patients. *J Neurosurg Spine* 2019;1-7.
- 11 Yu JH, Xu QH, Wang YH, Liao HF. Advances in the research and application of orbital blowout fracture repair material. *Zhonghua Yan Ke Za Zhi* 2019;55(11):876-880.
- 12 Homer N, Huggins A, Durairaj VD. Contemporary management of orbital blowout fractures. *Curr Opin Otolaryngol Head Neck Surg* 2019;27(4):310-316.
- 13 Tel A, Sembronio S, Costa F, Stenico AS, Bagatto D, D'Agostini S, Robiony M. Endoscopically assisted computer-guided repair of internal orbital floor fractures: an updated protocol for minimally invasive management. *J Cranio maxillofac Surg* 2019;47(12): 1943-1951.
- 14 Liao HF, Yu JH, Hu CQ, Hu XY, Liu Q, Wang YH, Wang AA, Xu QH. Application of three-dimensional printing combined with surgical navigation and endoscopy in orbital fracture reconstruction. *Zhonghua Yan Ke Za Zhi* 2019;55(9):658-664.
- 15 Zhang X, Chen W, Luo TY, Ma J, Dong Z, Cao G, Xu JK, Liu BY, Zhang QR, Zhang SL. Application of three-dimensional printing technology in the orbital blowout fracture reconstruction. *J Craniofac Surg* 2019;30(6):1825-1828.
- 16 Kim YC, Jeong WS, Park TK, Choi JW, Koh KS, Oh TS. The accuracy of patient specific implant prebent with 3D-printed rapid prototype model for orbital wall reconstruction. *J Craniomaxillofac Surg* 2017;45(6):928-936.
- 17 Tang C, Yang X, Gao Y, Zhang J, Xu LL, Zhang YQ. Clinical research on 3D printing technology for precise repair of orbital blowout fracture. *Journal of Precision Medicine* 2019;34(4):326-329.
- 18 Zhao QH, Gu JQ, Gao Y, Gao N, Wang RJ. Application value and prospect of 3D printing technology in medical field. *Machine Ddesign and Manufacturing Engineering* 2018;47(6):1-5.
- 19 Vijayavenkataraman S, Yan WC, Lu WF, Wang CH, Fuh JYH. 3D bioprinting of tissues and organs for regenerative medicine. *Adv Drug Deliv Rev* 2018;132:296-332.
- 20 Cheng BC, Jaffee S, Averick S, Swink I, Horvath S, Zhukauskas R. A comparative study of three biomaterials in an ovine bone defect model. *Spine J* 2020;20(3):457-464.
- 21 Oh JH, Kim HJ, Kim TI, Woo KM. Comparative evaluation of the biological properties of fibrin for bone regeneration. *BMB Rep* 2014;47(2):110-114.
- 22 Cao TQ, Cheng PZ, Yang L, Zhang SS, Li DL, Song Y, Liu B, Wu H, Pei GX. Experimental study on systemic biomechanics evaluation of rat femoral defect repair. *Chinese Journal of Orthopaedic Trauma* 2018;20(3):247-253.
- 23 Beamer B, Hettrich C, Lane J. Vascular endothelial growth factor: an essential component of angiogenesis and fracture healing. *HSS J* 2010;6(1):85-94.
- 24 Stegen S, van Gastel N, Carmeliet G. Bringing new life to damaged bone: the importance of angiogenesis in bone repair and regeneration. *Bone* 2015;70:19-27.
- 25 Keramaris NC, Calori GM, Nikolaou VS, Schemitsch EH, Giannoudis PV. Fracture vascularity and bone healing: a systematic review of the role of VEGF. *Injury* 2008;39(Suppl 2):S45-S57.
- 26 Geiger F, Lorenz H, Xu W, Szalay K, Kasten P, Claes L, Augat P, Richter W. VEGF producing bone marrow stromal cells (BMSC) enhance vascularization and resorption of a natural coral bone substitute. *Bone* 2007;41(4):516-522.
- 27 Becker R, Pufe T, Kulow S, Giessmann N, Neumann W, Mentlein R, Petersen W. Expression of vascular endothelial growth factor during healing of the meniscus in a rabbit model. *J Bone Joint Surg Br* 2004;86(7):1082-1087.
- 28 Al Subaie AE, Eimar H, Abdallah MN, Durand R, Feine J, Tamimi F, Emami E. Anti-VEGFs hinder bone healing and implant osseointegration in rat tibiae. *J Clin Periodontol* 2015;42(7): 688-696.
- 29 Orth M, Shenar AK, Scheuer C, Braun BJ, Herath SC, Holstein JH, Histing T, Yu XH, Murphy WL, Pohlemann T, Laschke MW, Menger MD. VEGF-loaded mineral-coated microparticles improve bone repair and are associated with increased expression of epo and RUNX-2 in murine non-unions. *J Orthop Res* 2019;37(4):821-831.
- 30 Ozturk BY, Inci I, Egri S, et al. The treatment of segmental bone defects in rabbit tibiae with vascular endothelial growth factor (VEGF)-loaded gelatin/hydroxyapatite "cryogel" scaffold. *Eur J Orthop Surg Traumatol* 2013;23(7):767-774.